

## Manifestations of geometric phase and enhanced spin Hall shifts in an optical trap

Basudev Roy<sup>1</sup>, Nirmalya Ghosh<sup>1</sup>, Ayan Banerjee<sup>1</sup>,  
Subhasish Dutta Gupta<sup>2</sup> and Soumyajit Roy<sup>3</sup>

<sup>1</sup> Department of Physical Sciences, IISER-Kolkata, Mohanpur 741252, India

<sup>2</sup> School of Physical Sciences, Hyderabad Central University, India

<sup>3</sup> EFAML, Materials Science Centre, Department of Chemical Sciences, IISER-Kolkata, Mohanpur 741252, India

E-mail: [nghosh@iiserkol.ac.in](mailto:nghosh@iiserkol.ac.in), [ayan@iiserkol.ac.in](mailto:ayan@iiserkol.ac.in) and [s.roy@iiserkol.ac.in](mailto:s.roy@iiserkol.ac.in)

Received 13 March 2014, revised 24 June 2014

Accepted for publication 26 June 2014

Published 21 August 2014

*New Journal of Physics* **16** (2014) 083037


doi:[10.1088/1367-2630/16/8/083037](https://doi.org/10.1088/1367-2630/16/8/083037)

### Abstract

The spin orbit interaction (SOI) of light has been the focus of recent research due to the fundamental consequences and potential applications in diverse systems, ranging from inhomogeneous anisotropic media to engineered plasmonics and metamaterial structures. Here, we demonstrate perhaps one of the simplest means to study SOI and the spin Hall shift (SHS) using a standard Gaussian TEM<sub>00</sub> beam in an optical trap. Our system exploits the versatility and interference generated in a stratified medium to control and manipulate SOI and transfer the resulting angular momentum to optically trapped microparticles. We show that even such a simple setup can lead to an order of magnitude enhancement in the SHS compared to the subwavelength shifts typically obtained. Importantly, this leads to the generation of doughnut-like mode structures from a fundamental Gaussian beam, as well as controlled rotation of mesoscopic particles using a linearly polarized Gaussian beam that lacks intrinsic angular momentum. The local optical torque leading to rotation of the particles is a direct measure of the local spin angular momentum (SAM) density of the field. Our measurement is the first experimental demonstration of using a probe particle to measure the SAM density for nonparaxial fields.



Content from this work may be used under the terms of the [Creative Commons Attribution 3.0 licence](https://creativecommons.org/licenses/by/3.0/). Any further distribution of this work must maintain attribution to the author(s) and the title of the work, journal citation and DOI.

 Online supplementary data available from [stacks.iop.org/njp/16/083037/mmedia](http://stacks.iop.org/njp/16/083037/mmedia)

Keywords: optical tweezers, angular momentum of light, geometric phase

Spin orbit interaction (SOI)—which couples the spin and orbital degrees of freedom of massive and massless particles—can be associated with several fundamental consequences in physics, including the fine and hyperfine structure in atoms [1] and the spin Hall effect (SHE) in electrons [2]. In the case of light, SOI and the accompanying geometric phases cause an interdependence of trajectory and polarization (spin). Thus, a change in the orbital degrees of freedom affects the polarization state of light and vice versa. The latter leads to the well-known SHE of light [3–9], whereas the former can lead to interconversion between the spin angular momentum (SAM) and the orbital angular momentum (OAM) of photons (spin–vortex coupling), polarization controlled vortices, and other intriguing effects of geometric phases in scattering and tight focusing [6, 10–15]. It is also pertinent to note that SHE and the spin–vortex coupling are interlinked, because the former is a consequence of total AM conservation [6]. In addition, experimental measurements of effects induced by SOI of light have helped aid in understanding quantum and condensed matter systems that have similar underlying physics. Although a few practical applications, such as nanodisplacement probes [9] and the generation of optical vortices [15], have been developed, in several cases, the effects of SOI have been rather small, with the magnitude of trajectory shifts reported due to the SHE of light typically being in subwavelength regimes [4–6]. However, in [9, 16], the SHE due to the scattering of nanoparticles was magnified using a focusing–imaging system with high numerical aperture (NA) microscope objectives so the extent of the SHE covered the exit pupil of the microscope.

Optical tweezers, which employ a tightly focused beam to trap and manipulate mesoscopic particles [17–21], have interesting consequences for SOI because tight focusing couples the trajectory and polarization of the propagating light. Indeed, the geometrical SHE of light has been experimentally studied by focusing through a truncated lens [22]. However, the only report of SOI in optical tweezers found in the literature is [10], where SOI-mediated angular momentum conservation was shown to affect the angular velocity of rotating birefringent particles for higher-order Gaussian beams. In this paper, we show that the strength of the SOI can be significantly magnified in a stratified medium used in the light path of the optical tweezers system. Note that tight focusing in a stratified medium has been theoretically studied previously [23]. However, these studies primarily addressed the effect of the stratified medium on the resulting intensity distribution of light. In addition, the results shown were for lenses with relatively low NA (around 0.9), and consequently, the focusing was not tight enough to produce any SOI effects. Thus, there could be no significant dependence of the intensity near the focus on the input polarization, which was therefore not considered in these studies. As we demonstrate in this paper, the situation is drastically modified for the use of high NA (1.4) microscope objectives in a stratified medium. This gives rise to enhanced SOI, which causes a large anisotropic linear diattenuation effect (differential attenuation of orthogonal polarizations) near the focal plane. Interestingly, we observe that, for a particular choice of layers for the stratified medium, a tightly focused linearly polarized Gaussian beam loses its azimuthal symmetry in the focal plane while side lobes are formed in the direction of the polarization. These side lobes become stronger as the beam propagates, so that at the region of caustics, the

beam splits into two with a definite azimuthal pattern. Further spatial evolution in the axial direction recovers the original Gaussian structure. Such polarization-dependent intensity distribution can be understood as a direct manifestation of the spin redirectional topological phase [8]. In addition, distinct regions of opposite ellipticity are produced at the edges of the intensity lobes as a manifestation of giant SHEs of light (more than  $2\lambda$  in magnitude). We perform a rigorous three-dimensional (3D) analysis of the polarization evolution to calculate the spin Hall shifts (SHS) near the focal plane and exploit the giant SHE to demonstrate experimentally the controllable rotation of asymmetric microparticles in the trap using only a fundamental Gaussian beam with no intrinsic angular momentum. In fact, the rotation of the particles corresponds to a direct measurement of the local SAM density of the field [24, 25]. Further, we believe this is the first instance this has been experimentally demonstrated for nonparaxial fields—measurements having been performed previously that consider the paraxial approximation of the field [26, 27].

## 1. Theory and simulations

It is now well understood that tight focusing of light leads to a longitudinal component that can be appropriately described using the framework of the Debye–Wolf theory [9, 16, 28, 29], which uses the plane wave (spatial harmonic) decomposition of the Gaussian beam. The evolution of each spatial harmonic can be represented by geometric rotations in the azimuthal ( $\phi$ ) and polar ( $\theta$ ) directions with respect to the laboratory frame. A transfer function is given  $A = R_z(-\phi)R_y(\theta)TR_z(\phi)$ , where  $R_i(\alpha)$  and  $i = x, y, z$  represents the SO(3) rotation matrix around the  $i$ -axis by an angle  $\alpha$  (for details, see supplementary information, available from [stacks.iop.org/njp/16/083037/mmedia](http://stacks.iop.org/njp/16/083037/mmedia)). The effects of the stratified medium for different polarizations of light are incorporated through the complex Fresnel transmission and reflection coefficients  $T_s(R_s)$  and  $T_p(R_p)$ , respectively. Note that, due to low index contrast, the total field in the stratified medium is dominated by the forward propagating waves. The final field inside the medium can be written as [35]

$$\begin{bmatrix} E_x^o \\ E_y^o \\ E_z^o \end{bmatrix} = C \begin{bmatrix} I_0 + I_2 \cos 2\psi & I_2 \sin 2\psi & 2iI_1 \cos \psi \\ I_2 \sin 2\psi & I_0 - I_2 \cos 2\psi & 2iI_1 \sin \psi \\ -2iI_1 \cos \psi & -2iI_1 \sin \psi & I_0 + I_2 \end{bmatrix} \begin{bmatrix} E_x^i \\ E_y^i \\ E_z^i \end{bmatrix} \quad (1)$$

where the superscripts  $i$  and  $o$  denote the input and output fields, respectively,  $I_0$ ,  $I_1$ , and  $I_2$  are the well-known diffraction integrals [35], and  $C$  is a constant. The effect of SOI is strongly manifested in the case of input linearly  $x$ -polarized light represented by a Jones vector  $[1 \ 0 \ 0]^T$ . Because linear polarization can be written as the sum of orthogonal circular polarizations, one would obtain right and left circularly polarized components that have OAM  $l = -2$  and  $l = 2$ , respectively, as well as linearly polarized longitudinal components with topological charge  $l = \pm 1$ , with each component satisfying total angular momentum conservation (see supplementary information). The generation of such circular polarization states from a linear input is a manifestation of the SHE. We will subsequently show that the effect of the stratified medium is to cause a giant SHE—or a transverse spatial shift of these individual polarization components so they have definite effects on trapped microparticles. It is also evident from equation (1) that the total intensity for incident linearly polarized light

would be given by

$$I(\rho) = |I_0|^2 + |I_2|^2 \pm 2 \mathbf{Re}(I_0 I_2^*) \cos 2\psi + 2|I_1|^2 (1 \pm \cos 2\psi). \quad (2)$$

Here, we introduce a quantity  $D$  where  $D = \mathbf{Re}(I_0 I_2^*) + |I_1|^2$ .  $D$  is known as the linear diattenuation parameter and is a measure of the polarization dependence of intensity, where the quantity  $D(1 \pm \cos 2\psi)$  gives the intensity distribution as a function of the input polarization angle  $\psi$ . Note that  $D(1 \pm \cos 2\psi)$  is essentially a geometric phase term that is picked up due to the SOI of the tightly focused light as it propagates through the stratified medium and its magnitude can be used to quantify the strength of SOI in the system.

It is important to note that the SHS originates because of the finite longitudinal component of the field that leads to transverse energy flows. This is manifested as transverse separation of the two constituent opposite circular polarization modes of the input linearly polarized state. The separation of the modes can be understood as the shift of the beam's center of gravity for the two opposite circular polarization states. Thus, the SHS can be determined from the longitudinal ( $P_z$ ) and the transverse ( $P_{x,y}$ ) components of the Poynting vector [12, 30, 31], so that a 3D treatment of polarization is warranted. Therefore, we proceed to build the 3D coherency matrix of the system [32, 33], from which we define the  $9 \times 1$  Stokes vectors  $\Lambda_{i,i=1,9}$  to include the longitudinal polarization component. Then, the total degree of polarization (DP) is defined as

$$\text{DP} = \frac{1}{3} \frac{\sum \Lambda_i^2}{\Lambda_o^2}, \quad (3)$$

so the degree of linear polarization (DLP) and degree of circular polarization (DCP) can be obtained from the corresponding linear and circular descriptor Stokes parameters. The helicity of the polarization is not apparent from the DP; thus, it is necessary to determine the two-dimensional (2D) DCP from the 2D Stokes vectors that are obtained by neglecting the  $z$ -components of the electric field in the 3D coherency matrix. This gives us the

$$\text{DCP} = \frac{V}{\sqrt{Q^2 + U^2 + V^2}}, \quad (4)$$

where  $Q$ ,  $U$ , and  $V$  are the well-known 2D Stokes vector elements (see supplementary information). Finally, the SHS for circularly polarized light is given by

$$\Delta y = \pm \frac{\Sigma y (P_x + P_y)}{\Sigma P_i}, \quad (5)$$

with the positive and negative signs corresponding to left and right circularly polarized light, respectively, and  $i = x, y, z$ . Now, for linearly polarized tightly focused light, the constituent circular polarization components evolve in different trajectories, which results in a net spatial shift of the individual components to create spatially separated regions of opposite circular polarization near the focal plane. We continue to show that this spatial separation, or SHS, is considerably amplified in the presence of a stratified medium leading to controlled rotation of asymmetric microparticles. It is also interesting to note that the torque on the particle resulting in its spinning motion is a direct measure of the SAM density of the field. The SAM density is given in Gaussian units by [24]

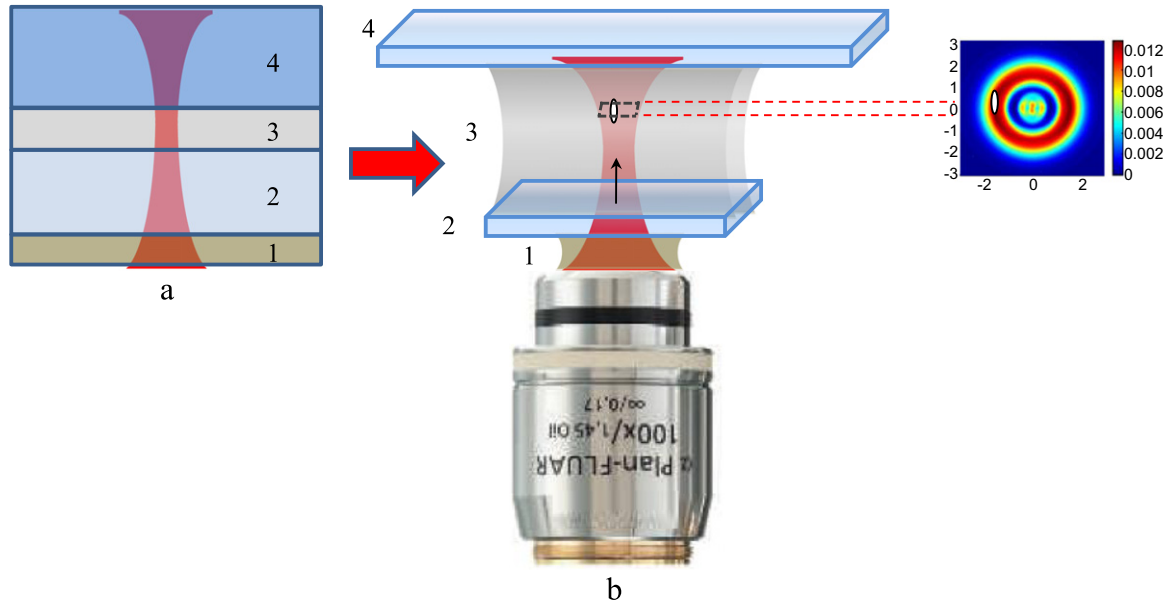


**Figure 1.** (a) Stratified medium (not to scale) formed in our experimental system with a Gaussian beam (direction shown) focused inside the sample solution. The various layers are (1) objective immersion oil (refractive index (RI) 1.516), (2) cover slip (RI 1.575), (aqueous solution of microparticles (RI) 1.33), and (4) top glass slide (RI 1.516). For conventional tweezers, the RI of (1) and (2) are matched. (b) A cartoon of the actual experimental setup with the different layers of stratified medium shown physically. The radial distribution of the electric field intensity near the focus (region shown using red dashed lines) is also shown. The intensity distribution is modified from a Gaussian structure into a ring-like pattern due to SOI.

$$\mathbf{S} = \frac{1}{16\pi\omega} \text{Im} [\mathbf{E}^* \times \mathbf{E} + \mathbf{H}^* \times \mathbf{H}], \quad (6)$$

which leads to a torque  $\mathbf{T} = \frac{1}{8\pi\omega} [\text{Im}(\alpha)\mathbf{S}]$ , where  $\omega$  is the frequency of the interacting light and  $\alpha$  is the polarizability of the particle [24]. However, because  $|\alpha_e| \gg |\alpha_m|$  usually ( $\alpha_e$  and  $\alpha_m$  are the electric and magnetic polarizabilities, respectively) it is the electric component of  $\mathbf{S}$  that interacts with the particle, which implies that the torque-producing rotation of the particle essentially measures the electric component of the SAM density. More specifically, any rotation in the radial direction is due to the  $z$ -component of the torque, which is proportional to  $(S_e)_z$ —the  $z$ -component of the electric SAM density—which, in turn, is proportional to DCP (equation (4)) modulated by the total intensity  $I(\rho)$  [24].

Using the preceding theoretical approach, we performed simulations for a stratified medium consisting of four layers that matched our experimental conditions. A schematic of our system is shown in figure 1(a). The optical tweezers are built around an inverted microscope (Zeiss Axiovert.A1) with a high NA objective (NA = 1.4) that tightly focuses the beam into the sample chamber, as shown in figure 1(b). The sample system consists of the following layers: (1) immersion oil, (2) cover slip, (3) sample aqueous solution and (4) glass slide. For the simulation, we selected two different RI values for layer 2 (cover slip). Simulations were completed for two specific cases, namely, (a) a perfectly polarizing cover slip ( $T_p = 0$ ,  $T_s \neq 0$ , RI = 1.575), which would lead to complete conversion of spin to OAM, and (b) partially polarizing cover slips ( $T_p, T_s \neq 0$ ) of different RI.

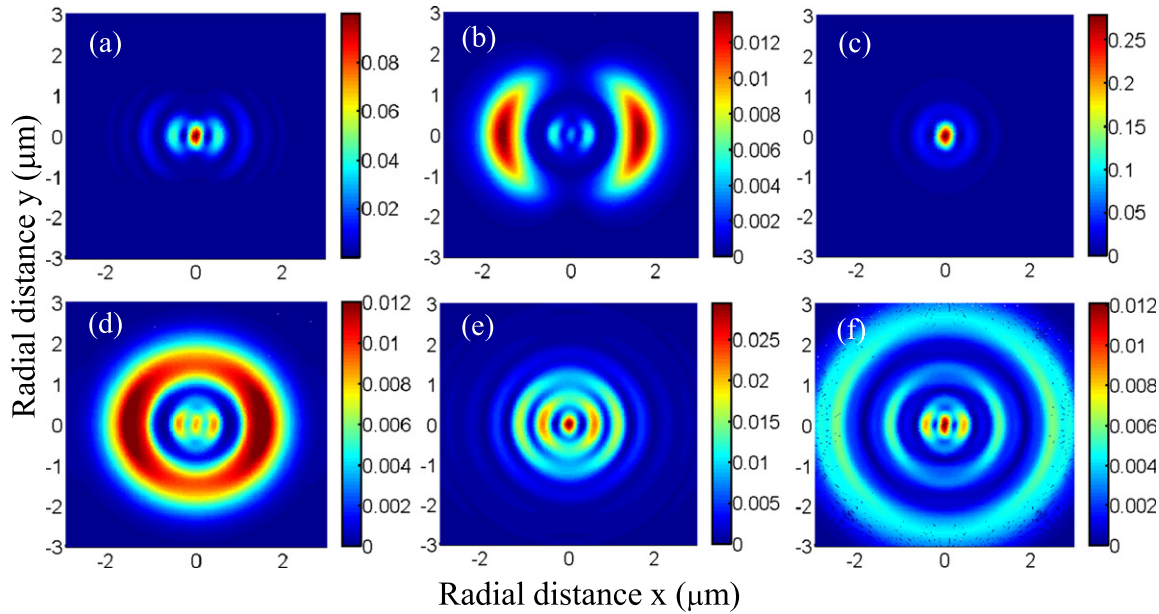


**Figure 2.** Intensity distributions inside sample chamber (layer 3 of figure 1) of trapping system for different RI and polarization properties of the cover slip (layer 2) for an  $x$ -polarized input beam. (a) Intensity distribution for polarized cover slip ( $T_p = 0$ ,  $T_s \neq 0$ ) with RI of 1.575, at the focus ( $z = 0$ ). Intensity side lobes, separated radially by around  $2 \mu\text{m}$ , with strength about 40% of that of the central lobe are seen. (b) Intensity distribution for same cover slip as in (a) at an axial distance  $2 \mu\text{m}$  away from the focus ( $z = 2$ ). The maximum intensity is now concentrated in two discrete side lobes formed opposite to each other in the direction of polarization of the input beam, and separated radially by around  $4 \mu\text{m}$ . (c) Intensity distribution at the focus for unpolarized ( $T_p \neq 0$ ,  $T_s \neq 0$ ) cover slip of RI 1.575 at the focus. Side lobes are absent. (d) Intensity distribution of same cover slip as in (c) at  $z = 2 \mu\text{m}$ . The side lobes in the polarization direction are present as in (b), but in the background of a continuous intensity ring of diameter about  $4 \mu\text{m}$  around the focus. (e) Intensity distribution for cover slip of RI 1.65 at  $z = 2 \mu\text{m}$ . Multiple rings are now visible within the diameter of  $3 \mu\text{m}$  that have higher intensity compared to (d). This implies a higher axial trapping depth as well as larger ring diameters for trapping of particles. (f) Intensity distribution for same cover slip of RI as in (e) at  $z = 3 \mu\text{m}$ . The ring diameter is now around  $5 \mu\text{m}$  with the intensity levels similar to (d).

It is observed that the enhanced SOI breaks down the azimuthal symmetry in the intensity profile so side lobes are formed even at the focus of the beam for a perfectly polarizing cover slip (figure 2(a)). These become stronger as the beam propagates axially so a doughnut profile is formed from an input Gaussian intensity distribution (figure 2(b)). For partially polarized cover slips (figures 2(c) and (d)), the side lobes appear in the background of an intensity ring, with the number of rings increasing with RI of the cover slip (figures 2(e) and (f)). Most importantly, the enhanced SOI results in a large SHS, manifested as spatially separated regions that have opposite circular polarization at the edges of the intensity lobes (figures 3(a)–(e)). Figure 3(f) shows the  $z$ -component of the electronic component of the SAM density ( $(S_e)_z$ ) for a polarized cover slip, whereas figure 3(g) shows the same for our experimental configuration (cover slip of RI 1.575) calculated from equation (6). An absorbing particle (shown as a white oval in figure 3(g)) trapped at such a region of high SAM density can experience a torque that may lead

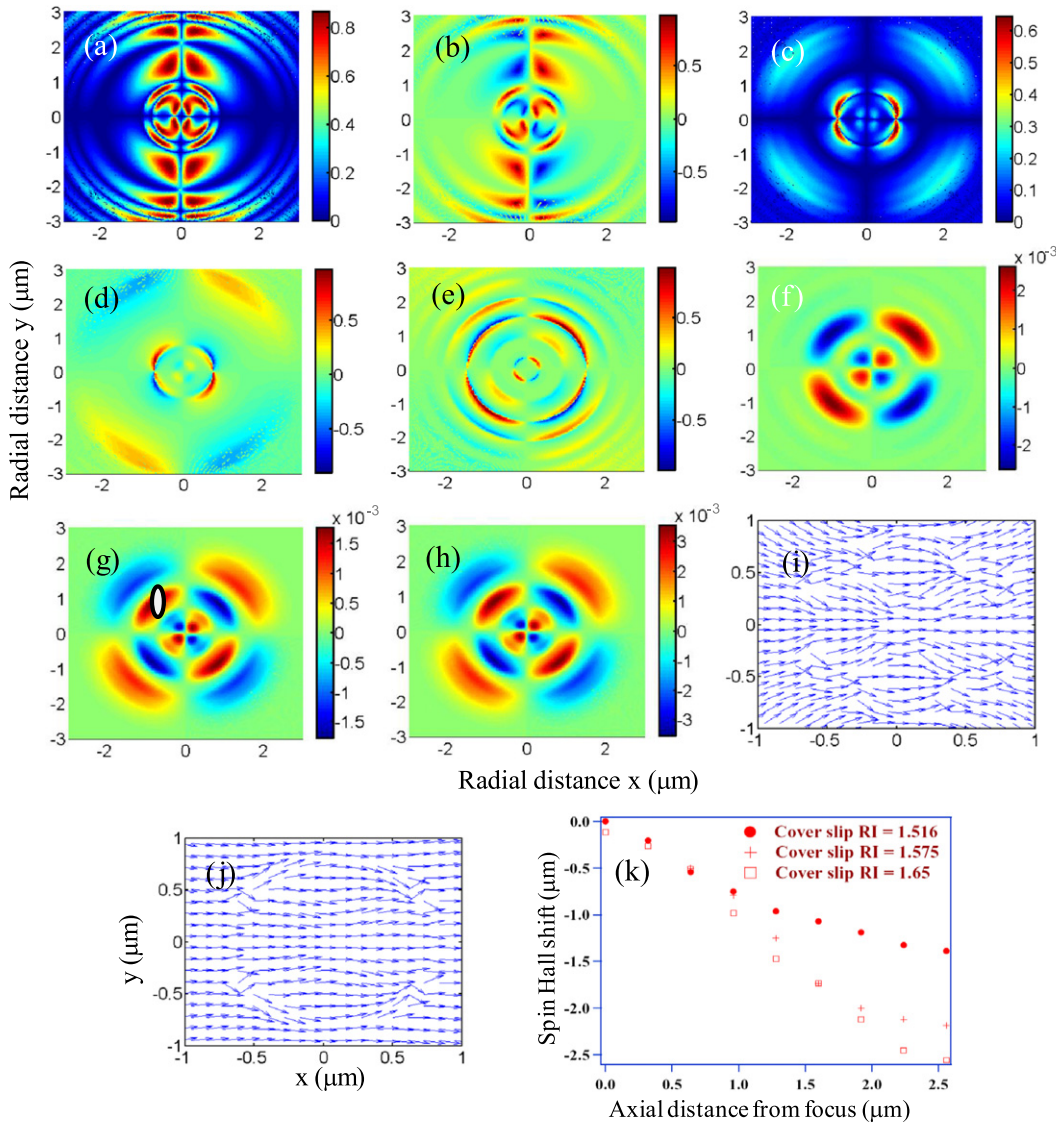


**Figure 3.** Study of polarization distributions inside sample chamber (layer 3 of figure 1) of trapping system for different RI and polarization properties of the cover slip (layer 2) for an  $x$ -polarized input beam. All data are for an axial plane  $2 \mu\text{m}$  away from the focus. (a) DP for polarized cover slip ( $T_p = 0$ ,  $T_s \neq 0$ ) with RI of 1.575. (b) DCP for (a). The helicities of the polarization lobes are now apparent. (c) DP for unpolarized cover slip with RI of 1.575. (d) DCP for (c). (e) DCP for RI=1.65. (f)  $(S_e)_z$  (equation (6)) for polarized cover slip. Note that the values in the color bar are in units of  $\frac{1}{16\pi\omega}$ . (g)  $(S_e)_z$  for our experimental case (RI=1.575). An asymmetric absorbing particle (white oval) trapped in the any of the high SAM regions would be likely to spin, the sense (clockwise or counterclockwise) dependent on the sign of the SAM density magnitude. (h) Total  $S_z$  (electric and magnetic components) for the experimental case. (i) Quiver plot showing the azimuth of the electric field vector for case (b). There are four regions in which the electric field describes a vortex; interspersed with these are regions of polarization singularity where the electric field does not exist. (j) Quiver plot showing the azimuth of the electric field vector for case (d). Vortex formation and polarization singularities are seen again, albeit over smaller regions compared to (g). (k) Plots of SHS against axial distance from the focus for layer 2 RIs = 1.516 (RI matched case with only one effective layer in the stratified medium), 1.575 and 1.65.

to spinning motion. It is also interesting to compare  $(S_e)_z$  with the total  $S_z$  (having both electric and magnetic components). Note that the electric and magnetic SAM densities may indeed be different for nonparaxial systems [24]. The difference may arise because of the presence of strong evanescent fields that could be created as a consequence of tight focusing through stratified media, or because of scattering from resonant Mie particles (selective excitation of transverse electric/transverse magnetic (TE/TM) scattering modes), excitation of surface plasmon polaritons, and so forth. However, because we use the conventional Debye–Wolf theory in our simulations, the inherent symmetry in the electric and magnetic fields leads to equal magnitudes of  $(S_e)_z$  and  $(S_m)_z$ , which is shown in figure 3(h). Here, we plot  $S_z$  for the experimental case and it is apparent that the radial distribution of the  $z$ -component of the total SAM remains unaltered with respect to that of the electric component (figure 3(g)), except for the magnitude, which is exactly doubled, thus implying that  $(S_e)_z = (S_m)_z$ . Note also that while  $(S_e)_z$  is proportional to the DCP, as is apparent from figures 3(c)–(g), there is a greater number of lobes in  $(S_e)_z$  because of the presence of the  $I(\rho)$  factor in  $(S_e)_z$ . As shown in figure 2, the distribution of  $I(\rho)$  coupled with that of the DCP produces the final radial profile of  $(S_e)_z$ , which shows more features than the DCP alone. In addition, tight focusing of input linearly polarized light also leads to the generation of phase vortices, which in turn creates polarization singularities close to the focus, as shown in figures 3(i) and (j). The azimuth of the electric field vector is calculated from  $\gamma = \frac{1}{2} \arctan\left(\frac{U}{Q}\right)$ , where  $U$  and  $Q$  are the well-known Stokes parameters. The magnitude of SHS (equation (5)) as a function of the axial distance also shows a definite tendency to increase with increasing RI of the cover slip, as observed from figure 3(k). Shifts of more than  $2\lambda$  obtained at an axial distance around  $2.5\ \mu\text{m}$  from the focus.

## 2. Experiment

We experimentally demonstrate the results of the effect of such large SOI and SHS on the mechanical motion of microparticles through a number of controlled experiments. A schematic of our setup is shown in figure 4(a). Images of the intensity distribution near the focal region confirm the results shown in figure 2(d) with a ring-like transverse pattern, which can lead to trapping of particles [34] and their movement along it [35]. We now exploit the large SHS produced in our system to induce a spinning motion in an individual trapped peapod-shaped soft oxometalate [36] or quartz microparticles (in accordance with the scheme displayed in figure 3(f)). The choice of asymmetric particles was driven by the fact that such particles exhibit form birefringence [37]. In the presence of elliptically polarized light, birefringent particles experience two types of torque—an alignment torque that aligns the fast axis of the particle along the electric field and a spinning torque proportional to the degree of ellipticity, light intensity, and thickness of the particle [38]. For purely circularly polarized light, the alignment torque vanishes and the particle exhibits pure rotation. We use two types of particles—peapod shaped soft oxometalates (ammonium phosphomolybdate,  $(\text{NH}_4)_3[\text{PMo}_{12}\text{O}_{40}]$ ) [36] of average dimension  $1.5 \times 0.5\ \mu\text{m}$  and quartz microparticles of generally arbitrary shape (obtained by crushing a large quartz crystal) but of dimensions between  $1\text{--}3\ \mu\text{m}$ . The experimental setup has been described in detail in [35]. The polarization of the beam can be controlled by a half-wave retarder placed at the input of the trap. As mentioned previously our cover slip is not index matched with the objective immersion oil, which is very different from standard optical



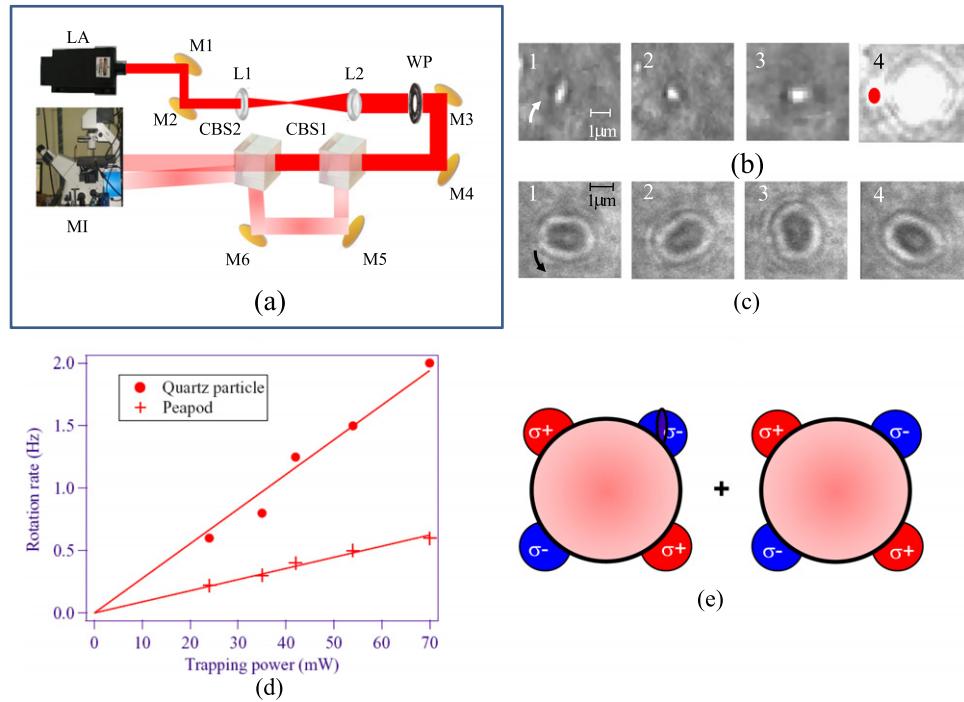


**Figure 4.** (a) Schematic of experimental setup—MI: inverted microscope; LA: solid state laser diode system at 1064 nm; M1-M6: mirrors; L1, L2: plano-convex lenses for beam size adjustment to overfill microscope back aperture; WP: linear (half-wave) wave-plate or retarder; CBS1, CBS2: 50–50 beam splitter cubes for 1064 nm. (b) Time series of a single trapped peapod rotating in the clockwise direction due to elliptical polarization created near the of  $f$ -axis intensity side lobes (see video 1 in the supplementary data). For trace 4, the IR filter in front of the camera has been removed and the particle is observed being trapped in the of  $f$ -axis intensity ring. (c) Time series of a single trapped ellipsoid shaped quartz particle rotating counterclockwise due to the same effect (see video 2 in the supplementary data). (d) Rotation speed versus trapping laser power for a representative peapod (red crosses) and quartz particle (red open circles). (e) Cartoon depicting the experimental design for control of rotation of a spinning particle. The particle (black transparent oval) spins in one of the ellipticity regions ( $\sigma^-$  in this case) produced due to SHS in the trapping light. A second beam of the same input polarization is introduced adjacent to the first beam so the ellipticity region nearest to the particle has opposite helicity of polarization. When the two spots are brought close together, the torque on the particle is canceled out if the intensities of the two beams are the same, which causes the particle to stop rotating, or reverses its direction of rotation if the intensity of the second beam is higher than the first beam, which produced higher opposite torque.

tweezers configurations and results in a stratified medium in the forward direction that enhances the SOI of the tightly focused trapping light. Note that the index mismatch could, in principle, be obtained using immersion oil that have different RI than the cover slip. However, previous studies we have published [35] show there is a crucial dependence of the index mismatched cover slip's thickness's effect in determining the intensity distribution near the trap focus. The thickness of oil (which is compressed between the microscope objective and cover slip, and is thus typically not more than 5–10  $\mu\text{m}$ ), even when it is index mismatched, will never be enough

to achieve the results that can be obtained using a cover slip that is more than 150  $\mu\text{m}$  (250  $\mu\text{m}$  in our case) thick.

In this work, we show the following distinct effects: (a) *rotation (spinning) of single particles using a linearly polarized Gaussian beam* and (b) *control of the rotation using a second beam*. We show the rotation of a single peapod (clockwise) and quartz particle (counterclockwise), respectively, in figures 4(b) and (c) (see also videos 1, 2 and 3 in the supplementary data, which show the clockwise and counterclockwise rotation of a peapod and counterclockwise rotation of a quartz particle, respectively). To visualize the particles, an IR filter is required in front of the camera to avoid saturating it. The filter is removed in image 4 in figure 4(a) where a ring-like intensity structure is evident from the rotating particle located on the ring at the left of the central maxima. This signifies that it is sampling a region of high ellipticity that causes it to spin (see video 1). Counterclockwise rotation of a peapod is shown in video 2, in which the peapod is now located at the right corner of the intensity ring (which is shown from the fact that the central maxima now appears at the left corner of the video). Figure 4(d) shows the rotation speed of a representative peapod (crosses) and quartz particle (open circles) as a function of incident laser power. The rotation frequencies of single trapped peapods and quartz particles are obtained by detecting the back-scattered intensity from a weak detection laser at 670 nm that is incident on the trapped particle. The output signal is modulated at the frequency of rotation. The quartz particles typically rotate faster (few Hz) because they are, on average, bigger and thicker than the peapods (sub-Hz rotation rate). Note that the torque particles are subjected to is actually a measurement of the local SAM density of the field.

Control of the rotation is demonstrated by introducing a second beam of the same polarization (see figure 4(e)), which can either stop the rotation or change the direction of rotation depending on its intensity with respect to the first beam. Thus, we use a nonpolarizing beam splitter cube at the input of the microscope to generate two independent trapping beams to form two traps adjacent to each other. The power levels of the two trapping beams are controlled by placing neutral density filters in the path of the beam reflected from the cube, as shown in figure 4(a). Videos 3 and 4 in the supplementary data demonstrate stopping and changing the direction of rotation of single quartz microparticles using the control beam, respectively.

### 3. Discussion

Spinning of particles about their axes has been reported in literature to be a consequence of the unbalanced torque arising due to the asymmetry in scattering from irregularly shaped particles [39]. For these cases, the asymmetry in the scattering must be strong enough to exceed the viscous drag force of the fluid medium that surrounds the particles. However, we have verified through simulation that such strong asymmetry does not arise for the ellipsoidal shaped particles that we observe rotating (figure 4(b) and (c)) in our experiments. Indeed, for scattering to cause rotations, the particles must have large extrusions on them to cause the strong azimuthal scattering asymmetry required to produce the necessary torque. Thus, we can safely conclude that the observed rotations on the particles are a consequence of the enhanced SOI.

It is crucial to note that the observed azimuthal asymmetry in the *radial distribution* of the intensity caused by SOI is very different from earlier studies on the *axial intensity distribution* near the focal plane of an optical trap due to change of focusing induced by the dielectric

interfaces encountered by the trapping beam [40–43]. This causes the well-known spherical aberration must be considered to calibrate the axial trapping force correctly [40]. On the other hand, the intensity and polarization distributions near the trap focus we have studied could be successfully exploited for inducing translatory motion [35], and controllable rotation (this work) in particles, and are unique manifestations of SOI and SHS.

We believe that our findings on the manifestations of the enhanced SOI due to the propagation of a tightly focused beam in a stratified medium could lead to further explorations on these systems. While we have experimentally demonstrated interesting applications in controlled rotation and transportation of microparticles, several other applications can also be envisaged that may open new research directions for research in optical tweezers. For example, microparticles can be trapped in multiple radial rings (figure 2(f)) similar to holographic tweezers, but using a single Gaussian beam. The presence of annular regions of high ellipticity could also produce multiparticle trapping in combination with rotations in both directions using a single Gaussian beam—a configuration that could enable the study of optical binding as well as exchange of angular momentum between birefringent particles. In addition, it may be interesting to study possible imbalances in the  $z$ -component of the electric and magnetic SAM densities in tight focusing through stratified media due to the effect of strong evanescent fields, or the presence of Mie scatterers and plasmonic structures interacting with the tightly focused light.

In conclusion, we investigated many interesting manifestations of SOI due to a tightly focused Gaussian beam propagating in a stratified optical trap. We studied the effects of both spin redirectional geometric phase and polarization dependent trajectory (SHE). The effect of the geometric phase was shown to introduce a large anisotropic diattenuation that modified the radial intensity distribution near the focal plane. For a cover slip chosen to be a polarizer for certain spatial harmonics, the structure of a Gaussian beam was modified to the extent of the formation of discrete of  $f$ -axis intensity lobes around the center at the focus. For partially polarizing cover slips, a high RI value caused the formation of intensity lobes in the background of a continuous ring that could be used to transport particles [35], as well as multiple intensity rings that could support the trapping of particles similar to holographic tweezers in the radial direction. The enhanced SOI also caused a large SHE to break down the incident linearly polarized Gaussian beam into components of large degree of opposite circular polarization that are spatially separated due to a large SHS near the trap focal plane. Asymmetric particles trapped at the epicentres of such regions can be rotated (spun) with full control on their rotational degree of freedom. The torque experienced by the particles is thus a measure of the electric component of the local SAM density of the optical field, and we believe this measurement is the first of its kind in using a microprobe to directly measure the SAM density of nonparaxial fields.

## Acknowledgments

The authors would like to acknowledge Arijit Haldar for the EM field analysis and Atharva Sahasrabuddhe and Bibudha Parasar for help in preparing the peapod and quartz samples. This work was supported by the Indian Institute of Science Education and Research, Kolkata, an autonomous research and teaching institute funded by the Ministry of Human Resource Development, Government of India. SR thanks DST Fast Track and BRNS DAE grants.

## References

- [1] Cohen-Tannoudji C, Diu B and Laloë F 2005 *Quantum Mechanics* vol 2 (Weinheim: Wiley-VCH)
- [2] Hirsch J E 1999 *Phys. Rev. Lett.* **83** 1834–7
- [3] Liberman V S and Zeldovich B Y 1992 *Phys. Rev. A* **46** 5199
- [4] Onoda M, Murakami S and Nagaosa N 2004 *Phys. Rev. Lett.* **93** 083901
- [5] Bliokh K, Nivi A, Kleiner V and Hasman E 2008 *Nat. Photon.* **2** 748
- [6] Bomzon Z and Gu M 2007 *Opt. Lett.* **32** 3017
- [7] Bliokh K and Desyatnikov A S 2009 *Phys. Rev. A* **79** 011807(R)
- [8] Bliokh K, Gorodetski Y, Kleiner V and Hasman E 2008 *Phys. Rev. Lett.* **101** 030404
- [9] Rodríguez-Herera O G, Lara D, Bliokh K Y, Ostrovskaya E A and Dainty C 2010 *Phys. Rev. Lett.* **104** 253601
- [10] Zhao Y, Scott Edgar J, Jeffries G D M, McGloin D and Chiu D T 2007 *Phys. Rev. Lett.* **99** 073901
- [11] Vuong L T, Adam A J L, Brok J M, Planken P C M and Urbach H P 2010 *Phys. Rev. Lett.* **104** 083903
- [12] Haefner D, Sukhov S and Dogariu A 2009 *Phys. Rev. Lett.* **102** 123903
- [13] Berry M V, Jeffrey M R and Mansuripur M 2005 *J. Opt. A* **7** 685
- [14] Marrucci L, Manzo C and Paparo D 2006 *Phys. Rev. Lett.* **96** 163905
- [15] Brasselet E 2009 *Phys. Rev. Lett.* **103** 103903
- [16] Bliokh K Y, Ostrovskaya E A, Alonso M A, Rodríguez-Herrera O G, Lara D and Dainty C 2011 *Opt. Express* **19** 26132
- [17] Irvine W T M, Hollingsworth A D, Grier D G and Chaikin P M 2013 *Proc. Natl Acad. Sci. USA* **110** 15544
- [18] Dholakia K and Ciz̄már T 2011 *Nat. Photon.* **5** 335–42
- [19] Fazal F M and Block S M 2011 *Nat. Photon.* **5** 318–21
- [20] Padgett M and Bowman R 2011 *Nat. Photon.* **5** 343
- [21] Wu T, Nieminen T A, Mohanty S, Miotke J, Meyer R L, Rubinsztein-Dunlop H and Berns M W 2012 *Nat. Photon.* **6** 262–7
- [22] Kundikova N D, Podgomov F V, Rogacheva L F and Ya Zeldovich B 1995 *Pure Appl. Opt.* **4** 179
- [23] Török P, Varga P and Booker G R 1995 *JOSA A* **12** 2136  
Török P and Varga P 1997 *Appl. Opt.* **36** 2305
- [24] Bliokh K Y, Bekshaev A Y and Nori F 2014 *Nat. Commun.* **5** 1
- [25] Canagauier-Durand A, Cuche A, Genet C and Ebbesen T W 2013 *Phys. Rev. A* **88** 033831
- [26] Garcés-Chávez V, McGloin D, Padgett M J, Dultz W, Schmitzer H and Dholakia K 2003 *Phys. Rev. Lett.* **91** 093602
- [27] O’Neil A T, MacVicar I, Allen L and Padgett M J 2002 *Phys. Rev. Lett.* **88** 053601
- [28] Born M and Wolf E 1989 *Principles of Optics* (Oxford: Pergamon)
- [29] Richards B and Wolf E 1959 *Proc. R. Soc. Lond. A* **253** 358
- [30] Arnoldus H F, Li X and Shu J 2008 *Opt. Lett.* **33** 1446
- [31] Bekshaev A 2011 *Ukr. J. Phys. Opt.* **12** 10
- [32] Ellis J, Dogariu A, Ponomarenko S and Wolf E 2002 *Opt. Commun.* **248** 333
- [33] Setälä T, Shevchenko A, Kaivola M and Friberg A T 2002 *Phys. Rev. E* **66** 016615
- [34] Haldar A, Pal S B, Roy B, Dutta Gupta S and Banerjee A 2012 *Phys. Rev. A* **85** 033832
- [35] Roy B, Ghosh N, Gupta S D, Panigrahi P K, Roy S and Banerjee A 2013 *Phys. Rev. A* **87** 043823
- [36] Roy S 2011 *Comm. Inorg. Chem.* **32** 113  
Roy S, Rijnveld-Ockers M T, Groenewold J, Kuipers B W M, Meeldijk H and Kegel W K 2007 *Langmuir* **23** 5292
- [37] Bohren C F and Huffman D R 2004 *Absorption and Scattering of Light by Small Particles* (Weinheim: Wiley-VCH)
- [38] Friese M E J, Nieminen T A, Heckenberg N R and Rubinsztein-Dunlop H 1998 *Nature* **394** 348

- 
- [39] Nieminen T A, Loke V L Y, Stilgoe A B, Knöner G, Branczyk A M, Heckenberg H R and Rubinsztein-Dunlop H 2007 *J. Opt. A* **9** S196
- [40] Dogariu A and Rajagopalan R 2000 *Langmuir* **16** 2770
- [41] Neves A A A, Fontes A, Cesar C L, Camposeo A, Cingolani R and Pisignano D 2007 *Phys. Rev. E* **76** 061917
- [42] Neuman K C, Abbondanzieri E A and Block S M 2005 *Opt. Lett.* **30** 1318
- [43] Roichman Y, Waldron A, Gardel E and Grier D G 2006 *Appl. Opt.* **45** 3425